

Article

Bi₂O₃-Assisted Sintering of Na₃Zr₂Si₂PO₁₂ Electrolyte for Solid-State Sodium Metal Batteries

 Shangxu Cen ¹, Wentao Mei ¹, Xiangyuan Xing ¹, Yiwei Zeng ², Zhiyong Mao ² , Dajian Wang ², Jingjing Chen ^{2,*} and Chenlong Dong ^{1,*}
¹ Tianjin Key Laboratory for Photoelectric Materials and Devices, School of Materials Science and Engineering, Tianjin University of Technology, Tianjin 300384, China

² School of Science, Tianjin University of Technology, Tianjin 300384, China

* Correspondence: cj313313@email.tjut.edu.cn (J.C.); dongchenlong@email.tjut.edu.cn (C.D.)

Abstract: Solid-state sodium metal batteries using non-flammable solid-state electrolytes are recognized as next-generation energy storage technology in view of their merits of high safety and low cost. However, the lower ion conductivity (below the application requirements of 10^{-3} S cm⁻¹) and interface issues that exist in electrolytes/electrodes for most solid-state electrolytes hinder their practical application. In this paper, NASICON-type Na₃Zr₂Si₂PO₁₂ (NZSP) electrolytes with enhanced ion conductivity are synthesized by the Bi₂O₃-assisted sintering method. The influence of the Bi₂O₃ sintering agent content on the crystalline phase, microstructure, density and ion conductivity as well as the electrochemical performances applied in batteries for the obtained NZSP electrolytes are investigated in detail. With the presence of Bi₂O₃, the formed Na₃Bi(PO₄)₂ impurity increased the Si/P ratio in the NASICON structure with higher Na⁺ occupancy, then enhanced the ionic conductivity to a level of 1.27×10^{-3} S cm⁻¹. Unfortunately, the Bi₂O₃-assisted sintered NZSP shows a degradation in the cycling stability when applied to solid-state sodium batteries because of the decreased interfacial stability with Na anodes. The formation of a Bi-Na alloy during cycling might be conducive to Na dendrite growth in electrolytes, degrading the cycling performance. This work presents a facial method to improve the ion conductivity of NASICON-type electrolytes and gives insight into the interface issues of solid-state sodium metal batteries.

Keywords: solid-state sodium metal batteries; NASICON-type electrolyte; ion conductivity; interface



Citation: Cen, S.; Mei, W.; Xing, X.; Zeng, Y.; Mao, Z.; Wang, D.; Chen, J.; Dong, C. Bi₂O₃-Assisted Sintering of Na₃Zr₂Si₂PO₁₂ Electrolyte for Solid-State Sodium Metal Batteries. *Coatings* **2022**, *12*, 1774. <https://doi.org/10.3390/coatings12111774>

Academic Editor: Alessandro Latini

Received: 8 October 2022

Accepted: 14 November 2022

Published: 20 November 2022

Publisher's Note: MDPI stays neutral with regard to jurisdictional claims in published maps and institutional affiliations.



Copyright: © 2022 by the authors. Licensee MDPI, Basel, Switzerland. This article is an open access article distributed under the terms and conditions of the Creative Commons Attribution (CC BY) license (<https://creativecommons.org/licenses/by/4.0/>).

1. Introduction

Sodium-ion batteries are recognized as promising next-generation energy storage technology due to their merits of low cost and an abundance of sodium resources compared to traditional lithium ion batteries [1,2]. Similar to conventional lithium-ion batteries, sodium-ion batteries use organic liquid electrolytes to show potential safety hazards such as combustion and explosion. Alternatively, solid-state sodium metal batteries employing solid-state electrolytes and sodium metal anodes can effectively solve the safety issues originating from organic liquid electrolytes and highly improve the energy density of devices [3,4]. In view of their excellent structural and chemical stability, high ionic conductivity ($>10^{-4}$ S cm⁻¹) and wide electrochemical window (>5 V), NASICON-type solid electrolytes have received abundant research attention in recent years [5,6]. As a typical NASICON structure, Na₃Zr₂Si₂PO₁₂ (NZSP) was firstly exploited in 1976 by Hong and Goodenough and reported widely owing to its relative higher ionic conductivity [7,8]. Nevertheless, the ionic conductivity of NZSP electrolyte is still lower than that of the liquid electrolyte organic (10^{-3} – 10^{-2} S cm⁻¹) [9]. In addition, the poor contact between rigid NZSP electrolytes and electrodes results in large interfacial impedance and the growth of dendrites as well as other interfacial issues. Therefore, improving the ionic conductivity of NZSP electrolytes and effectively solving the interface problem are the top priorities for the practical application of NZSP in solid-state metal sodium batteries.

The ionic conductivity of a NASICON electrolyte is determined by several factors, such as the number and distribution of Na ions, phase structure as well as the relative density. The most commonly used strategy to improve the ion conductivity of a NZSP electrolyte is the partial substitution of Zr^{4+} in a $Na_3Zr_2Si_2PO_{12}$ structure by variable heterogeneous ions [10]. For example, Lu et al. reported that the mobility of Na^+ at the Na3 site could be promoted by doping 5 at% Ca^{2+} , leading to an enhanced ionic conductivity of $1.67 \times 10^{-3} S cm^{-1}$ [11]. Yang et al. employed Mg^{2+} as the substitution ion for Zr^{4+} by the means of non-equivalent substitution to generate a deficiency in positive charge and then to increase the concentration of Na^+ , resulting in higher ion conductivity at $1.33 \times 10^{-3} S cm^{-1}$ [12]. Zhang et al. introduced La^{3+} into a Zr^{4+} site to form a new $Na_3La(PO_4)_2$ phase, which not only improved the Na^+ concentration in the $Na_3Zr_2Si_2PO_{12}$ ($3.4 \times 10^{-3} S cm^{-1}$) but also increased the relative density [13]. Miao R et al. reported the influence of a Bi_2O_3 additive on the electrochemical performance of $Na_{3.1}Y_{0.1}Zr_{1.9}Si_2PO_{12}$ inorganic solid electrolytes [14]. We summarize the ionic conductivities of NASICON electrolytes with different ionic dopants in Table 1.

Table 1. The ionic conductivities of previously reported NASICON electrolytes with different dopants at room temperature.

Components	Ionic Conductivity ($S cm^{-1}$)	Reference
$Na_3Zr_{1.9}Ca_{0.1}Si_2PO_{12}$	1.67×10^{-3}	[11]
$Na_3Zr_{1.7}La_{0.3}Si_2PO_{12}$	3.4×10^{-3}	[13]
$Na_{3.1}Y_{0.1}Zr_{1.9}Si_2PO_{12} + 1 wt.\% Bi_2O_3$	1.21×10^{-3}	[14]
$Na_3Zr_{1.9}Nb_{0.1}Si_2PO_{12}$	2.11×10^{-4}	[15]
$Na_3Zr_{1.9}Ti_{0.1}Si_2PO_{12}$	5.97×10^{-4}	[15]
$Na_3Zr_{1.8}Zn_{0.2}Si_2PO_{12}$	2.50×10^{-3}	[15]
$Na_3Zr_{1.9}Yb_{0.1}Si_2PO_{12}$	1.7×10^{-4}	[16]
$Na_3Zr_{1.9}Gd_{0.1}Si_2PO_{12}$	6.0×10^{-4}	[16]
$Na_3Zr_{1.9}Ce_{0.1}Si_2PO_{12}$	9.0×10^{-4}	[16]
$Na_3Zr_{1.9}Al_{0.1}Si_2PO_{12}$	4.39×10^{-4}	[17]
$Na_3Zr_{1.9}Fe_{0.1}Si_2PO_{12}$	7.53×10^{-4}	[17]
$Na_3Zr_{1.9}Co_{0.1}Si_2PO_{12}$	1.55×10^{-4}	[17]
$Na_3Zr_{1.9}Ni_{0.1}Si_2PO_{12}$	6.18×10^{-4}	[17]
$Na_3Zr_{1.9}Ga_{0.1}Si_2PO_{12}$	1.06×10^{-3}	[18]
$Na_{3.4}Zr_{1.6}Sc_{0.4}Si_2PO_{12}$	4.0×10^{-3}	[19]
$Na_{3.1}Zr_{1.95}Mg_{0.05}Si_2PO_{12}$	3.5×10^{-3}	[20]
$Na_{3.2}Zr_{1.8}Sm_{0.2}Si_2PO_{12}$	1.36×10^{-3}	[21]
$Na_{3.3}Zr_{1.7}Ho_{0.3}Si_2PO_{12}$	1.07×10^{-3}	[21]
$Na_{3.33}Ce_{0.02}Sc_{0.33}Zr_{1.65}Si_2PO_{12}$	2.44×10^{-3}	[22]
$Na_{2.9}K_{0.1}Zr_2Si_2PO_{12}$	7.734×10^{-4}	[23]
$Na_{3.4}Zr_2Si_2P_{0.6}O_{12}$	5.5×10^{-3}	[24]
$Na_{3.4}Zr_{1.9}Mg_{0.1}Si_{2.2}P_{0.8}O_{12}$	3.6×10^{-3}	[25]
$Na_3Zr_2Si_2PO_{12} + 5 wt.\% Na_2SiO_3$	1.45×10^{-3}	[26]
$Na_{3.2}Zr_2Si_2P_{0.8}O_{12} + 0.5 NaF$	3.6×10^{-3}	[27]

In this study, the Bi_2O_3 with a low melting point ($825^\circ C$) was introduced into the sintering process of a NASICON ($Na_3Zr_2Si_2PO_{12}$) solid electrolyte so as to create liquid flux at high temperatures and improve the relative density of the electrolyte pellet. After the introduction of Bi_2O_3 , the new phase of $Na_3Bi(PO_4)_2$ was generated at the grain boundary, which altered the Si/P ratio of $Na_3Zr_2Si_2PO_{12}$ phase and further enhanced the Na^+ occupancy. The optimized ionic conductivity of $Na_3Zr_2Si_2PO_{12}$ -Bi is $1.27 \times 10^{-3} S cm^{-1}$, which is much higher than that of pure $Na_3Zr_2Si_2PO_{12}$ ($2.84 \times 10^{-4} S cm^{-1}$). However, the direct contact of Na with $Na_3Zr_2Si_2PO_{12}$ -Bi triggers the formation of a Na_xBi alloy at the metal/electrolyte interface, which accelerates the dendrite growth of Na inside the electrolyte pellets. Such Na penetration into the electrolyte prompts the decreased electrochemical performance of the symmetrical battery and the solid sodium metal full bat-

tery. We believe the electrochemical performance of $\text{Na}_3\text{Zr}_2\text{Si}_2\text{PO}_{12}$ -Bi-based solid sodium metal batteries can be further enhanced by a physical obstruction between Na metal and $\text{Na}_3\text{Zr}_2\text{Si}_2\text{PO}_{12}$ -Bi electrolyte.

2. Materials and Methods

The $\text{Na}_3\text{Zr}_2\text{Si}_2\text{PO}_{12-x}\text{Bi}$ ($\text{Na}_{3+x}\text{Zr}_{2-x}\text{M}_x\text{Si}_2\text{PO}_{12}$, $x = 0, 0.1, 0.2, 0.3$ and 0.4) was synthesized by conventional high-temperature solid-state reaction. Stoichiometric amounts of Na_2CO_3 , $\text{NH}_4\text{H}_2\text{PO}_4$, ZrO_2 , SiO_2 and Bi_2O_3 were mixed by high-energy ball milling for 1 h at a rotating speed of 1400 rpm and then calcinated at $1100\text{ }^\circ\text{C}$ for 12 h. The 15%-excessive Na_2CO_3 and $\text{NH}_4\text{H}_2\text{PO}_4$ were added to compensate for the volatilization of Na and P. After ball milling, the obtained mixture was further ball-milled for 1 h. The resultant dry powder was sieved through a 200-mesh sieve, then mixed with PVA binder and pressed into green pellets with a diameter of 16 mm and a thickness of 1 mm. The green pellets were pre-calcinated at $650\text{ }^\circ\text{C}$ for 2 h to remove the PVA binder and finally calcinated at $1200\text{ }^\circ\text{C}$ for 12 h to obtain dense electrolyte pellets.

The phase composition of $\text{Na}_3\text{Zr}_2\text{Si}_2\text{PO}_{12-x}\text{Bi}$ was confirmed by X-ray diffractometer (ARL Equinox 3000, Thermo Fisher, MA, USA). The microstructure was observed by scanning electron microscope (Quanta FEG, FEI, NY, USA) equipped with energy dispersive X-ray spectroscopy. The relative density of electrolyte pellets was measured by electronic densitometer (YD-100ES, YiEnDa, China) based on the Archimedes principle. The ionic and electronic conductivities were tested on electrochemical station (CHI 760E). The blocking electrode was constructed by sputtering Au on two sides of electrolyte pellets. The ionic conductivity was determined by electrochemical impedance spectroscopy (EIS, CHI 760E, ChenHua, Shanghai, China) technique ranging from 100 kHz to 0.1 Hz with an amplitude of 5 mV under open circuit potential. The electronic conductivity was determined by the DC polarization method at a constant voltage of 0.1–1.8 V for 1800 s at room temperature.

Sodium foils with a diameter of 8 mm were attached to both sides of the polished electrolyte sheet and then repetitively rolled to modify the interfacial contact. The Na/ $\text{Na}_3\text{Zr}_2\text{Si}_2\text{PO}_{12}$ /Na and Na/ $\text{Na}_3\text{Zr}_2\text{Si}_2\text{PO}_{12-x}\text{Bi}$ /Na symmetric batteries were assembled into CR2032 coin cell to investigate the Na plating/stripping behaviors in an argon-filled glove box at room temperature. Critical current measurements were performed by the galvanostatic cycling at current densities stepping from 0.1–0.6 mA cm^{-2} (step: 0.05 mA cm^{-2} , time: 0.5 h) at room temperature. The CR2032 full battery was assembled using sodium foil as the anode, NZSP pellet as the electrolyte and NVP as the cathode material in an argon-filled glove box at room temperature. Commercial $\text{Na}_3\text{V}_2(\text{PO}_4)_3$ (Hubei Energy Technology Co., Ltd.), acetylene black and poly(vinylidene fluoride) (PVDF) with a weight ratio of 8:1:1 were mixed in N-methyl pyrrolidone (NMP) to form a homogeneous slurry, ergo coated on aluminum foil by doctor blade and finally dried at $120\text{ }^\circ\text{C}$ for 24 h in vacuum oven. The mass loading of NVP was $\sim 1\text{ mg cm}^{-2}$. Ten μL of liquid electrolytes (1 M NaClO_4 in EC/DMC (1:1) + 5% FEC) was added between cathode and electrolyte pellet to establish wetted interface.

3. Results and Discussion

Figure 1a displays the XRD pattern of solid electrolytes of $\text{Na}_3\text{Zr}_2\text{Si}_2\text{PO}_{12}$, which is sintered at $1200\text{ }^\circ\text{C}$. The diffraction peaks of $\text{Na}_3\text{Zr}_2\text{Si}_2\text{PO}_{12}$ can be owned as NASICON structures (PDF #84-1200), as shown in Figure 1b. A small amount of ZrO_2 impurity can be found because of the excessive volatilization of Na and P during the high-temperature sintering process [13], while for $\text{Na}_3\text{Zr}_2\text{Si}_2\text{PO}_{12-x}\text{Bi}$ ($x = 0, 0.1, 0.2, 0.3$, and 0.4) samples, it is obvious that the Bi_2O_3 addition can facilitate the crystallization of $\text{Na}_3\text{Zr}_2\text{Si}_2\text{PO}_{12}$ and decrease the formation of ZrO_2 impurities. With enhanced Bi_2O_3 contents, especially for $x > 0.3$, the intensity of the ZrO_2 impurities gradually enhances. Moreover, the introduction of Bi_2O_3 induces the generation of the $\text{Na}_3\text{Bi}(\text{PO}_4)_2$ phase, as confirmed by the characteristic peaks located at 21.5° , 25.5° , 32.2° and 33.6° (PDF #81-0336). Because the formation of $\text{Na}_3\text{Bi}(\text{PO}_4)_2$ phase is cause by the solid-state reaction of Bi_2O_3 , Na_2CO_3 and $\text{NH}_4\text{H}_2\text{PO}_4$, the generation of the $\text{Na}_3\text{Bi}(\text{PO}_4)_2$ phase can increase the Si/P ratio of the NASICON struc-

ture and enhance the Na^+ occupancy, which may contribute to enhanced ionic conductivity. To investigate the origin of $\text{Na}_3\text{Bi}(\text{PO}_4)_2$ formation, the solid-state reaction of Na_2CO_3 , $\text{NH}_4\text{H}_2\text{PO}_4$ and Bi_2O_3 was proceeded at 800°C . As shown in Figure 1c, the XRD pattern can be indexed as the pure $\text{Na}_3\text{Bi}(\text{PO}_4)_2$ phase (PDF #81-0036) [28]. Therefore, before the phase formation of $\text{Na}_3\text{Zr}_2\text{Si}_2\text{PO}_{12}$, parts of Bi_2O_3 were converted into $\text{Na}_3\text{Bi}(\text{PO}_4)_2$, and the remaining Bi_2O_3 melted at a high temperature and was substituted for the Zr^{4+} site of $\text{Na}_3\text{Zr}_2\text{Si}_2\text{PO}_{12}$.

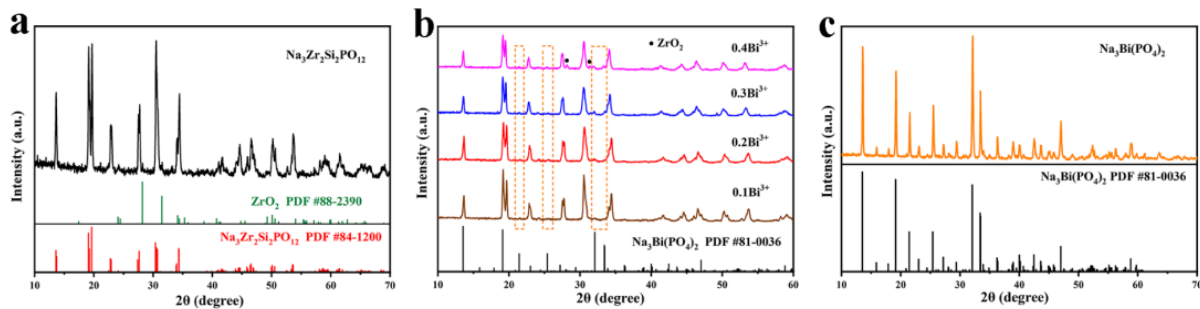


Figure 1. XRD patterns of (a) $\text{Na}_3\text{Zr}_2\text{Si}_2\text{PO}_{12}$, (b) $\text{Na}_3\text{Zr}_2\text{Si}_2\text{PO}_{12-x}\text{Bi}$ ($x = 0, 0.1, 0.2, 0.3$ and 0.4) and (c) $\text{Na}_3\text{Bi}(\text{PO}_4)_2$.

According to the Archimedes principle, the relative densities of $\text{Na}_3\text{Zr}_2\text{Si}_2\text{PO}_{12-x}\text{Bi}$ ($x = 0, 0.1, 0.2, 0.3, 0.4$) are 2.89, 3.07, 3.10, 3.08 and 3.02 g cm^{-3} , corresponding to the relative densities of 89.2, 94.8, 95.7, 95.1 and 93.2 %, respectively (Table 1). To investigate the effects of the Bi_2O_3 addition on the morphology of $\text{Na}_3\text{Zr}_2\text{Si}_2\text{PO}_{12}$ electrolytes, scanning electron microscopy (SEM) has been performed on the $\text{Na}_3\text{Zr}_2\text{Si}_2\text{PO}_{12-x}\text{Bi}$ ($x = 0, 0.1, 0.2, 0.3, 0.4$) samples, as shown in Figure 2. The grain size of the initial $\text{Na}_3\text{Zr}_2\text{Si}_2\text{PO}_{12}$ sample is large and variable, and there are plenty of holes between the grains. The relative density of a $\text{Na}_3\text{Zr}_2\text{Si}_2\text{PO}_{12}$ pellet is 89.2 %. When $x = 0.1$ and 0.2 , the grain size of $\text{Na}_3\text{Zr}_2\text{Si}_2\text{PO}_{12}$ particles becomes smaller and uniform, and there are no obvious gaps or holes observed. The highest relative density for a $\text{Na}_3\text{Zr}_2\text{Si}_2\text{PO}_{12-0.2}\text{Bi}$ sample is 95.7%. As is known, Bi_2O_3 is a typical low melting point oxide (825°C), which forms liquid flux at high temperatures and bonds the grain together, enabling enhanced crystallization and densification rates during sintering [28]. When $x = 0.3$ and 0.4 , the grain size of $\text{Na}_3\text{Zr}_2\text{Si}_2\text{PO}_{12}$ particles further decreases, and thereupon, a small number of gaps and holes reappear between the grains, which weakens the density.

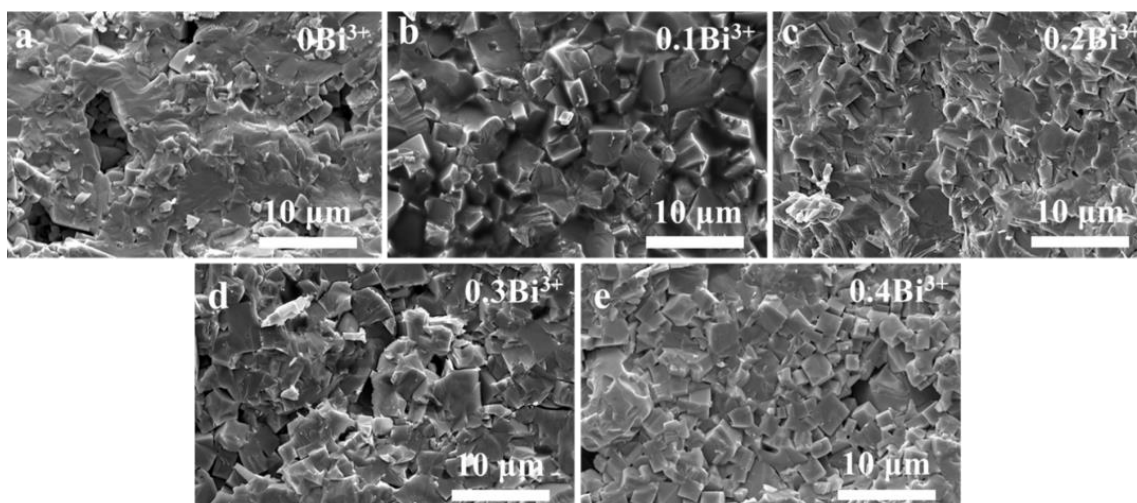


Figure 2. Top-view SEM images of $\text{Na}_3\text{Zr}_2\text{Si}_2\text{PO}_{12}$ samples with different Bi^{3+} concentrations: (a) zero, (b) 0.1, (c) 0.2, (d) 0.3 and (e) 0.4.

Figure 3a displays the EIS profiles of $\text{Na}_3\text{Zr}_2\text{Si}_2\text{PO}_{12-x}\text{Bi}$ ($x = 0, 0.1, 0.2, 0.3, 0.4$) at room temperature. The EIS curve consists of a semicircle in the high-frequency region and an inclined line in the low-frequency region [28]. The intersection of the semicircle's destination and the inclined line (Z' -intercept) is the total resistance of an electrolyte pellet. After Bi_2O_3 introduction, the total resistance and the radius of the semicircle in the high-frequency region decrease obviously, demonstrating a decreased total resistance. Moreover, the total resistance is composed of grain resistance (R_g) and grain boundary resistance (R_{gb}) [29]. The R_g and R_{gb} of $\text{Na}_3\text{Zr}_2\text{Si}_2\text{PO}_{12-x}\text{Bi}$ samples are obtained by fitting the EIS curve (Figure 3b), and the corresponding results have been summarized in Table 2.

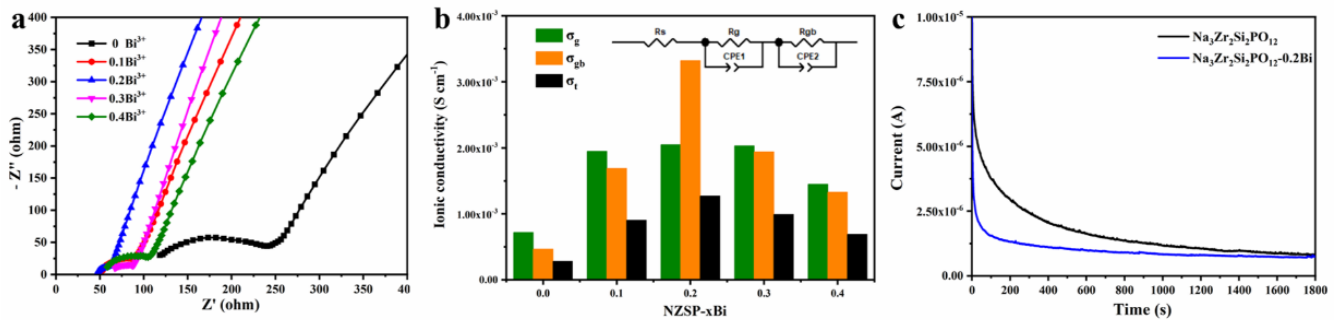


Figure 3. (a) Nyquist plots (b) Grain resistance, grain boundary resistance and total resistance of $\text{Na}_3\text{Zr}_2\text{Si}_2\text{PO}_{12-x}\text{Bi}$ ($x = 0, 0.1, 0.2, 0.3, 0.4$) samples at room temperature. (c) Polarization current–time curves at 1 V of $\text{Na}_3\text{Zr}_2\text{Si}_2\text{PO}_{12}$ and $\text{Na}_3\text{Zr}_2\text{Si}_2\text{PO}_{12-0.2}\text{Bi}$.

Table 2. Density and conductivity of $\text{Na}_3\text{Zr}_2\text{Si}_2\text{PO}_{12-x}\text{Bi}$ samples ($x = 0, 0.1, 0.2, 0.3$ and 0.4) at room temperature.

NZSP- x Bi	ρ (g cm^{-3})	R_g (Ω)	R_{gb} (Ω)	σ_b (S cm^{-1})	σ_{gb} (S cm^{-1})	σ_{total} (S cm^{-1})
$x = 0$	2.89	95.0	146.0	7.20×10^{-4}	4.69×10^{-4}	2.84×10^{-4}
$x = 0.1$	3.07	40.0	46.0	1.95×10^{-3}	1.69×10^{-3}	9.04×10^{-4}
$x = 0.2$	3.10	38.4	23.7	2.05×10^{-3}	3.32×10^{-3}	1.27×10^{-3}
$x = 0.3$	3.08	42.5	44.5	2.03×10^{-3}	1.94×10^{-3}	9.92×10^{-4}
$x = 0.4$	3.02	50.3	54.7	1.45×10^{-3}	1.33×10^{-3}	6.92×10^{-4}

The total ionic conductivities of $\text{Na}_3\text{Zr}_2\text{Si}_2\text{PO}_{12-x}\text{Bi}$ ($x = 0, 0.1, 0.2, 0.3, 0.4$) are 2.84×10^{-4} , 9.04×10^{-4} , 1.27×10^{-3} , 9.92×10^{-4} and 6.92×10^{-4} , respectively. When $x \leq 0.2$, the grain boundary conductivity grows significantly faster than the grain conductivity. When $x = 0.2$, the grain boundary conductivity ($\sigma_{gb} = 3.32 \times 10^{-3} \text{ S cm}^{-1}$) exceeds the grain conductivity ($\sigma_b = 2.05 \times 10^{-3} \text{ S cm}^{-1}$). The increasing of the grain conductivity originates from the enhanced density and the generation of $\text{Na}_3\text{Bi}(\text{PO}_4)_2$ phase, which increases the Si/P ratio and Na^+ occupancy of $\text{Na}_3\text{Zr}_2\text{Si}_2\text{PO}_{12}$ [30,31]. The increasing of the grain boundary conductivity is attributed to the reduction of gaps and pores between grains. when $x \geq 0.2$, σ_g and σ_{gb} simultaneously decrease, and the σ_{gb} is smaller than σ_g . The reason why σ_{gb} is smaller than σ_g is the formation of insulating ZrO_2 impurity, which hinders the Na^+ transport between $\text{Na}_3\text{Zr}_2\text{Si}_2\text{PO}_{12}$ grains [32]. Figure 3c shows the i - t curves of $\text{Na}_3\text{Zr}_2\text{Si}_2\text{PO}_{12}$ and $\text{Na}_3\text{Zr}_2\text{Si}_2\text{PO}_{12-0.2}\text{Bi}$ pellets under a fixed voltage of 1 V. The measured steady-state currents are $8.48 \times 10^{-7} \text{ A}$ for $\text{Na}_3\text{Zr}_2\text{Si}_2\text{PO}_{12}$ and $7.35 \times 10^{-7} \text{ A}$ for $\text{Na}_3\text{Zr}_2\text{Si}_2\text{PO}_{12-0.2}\text{Bi}$. Correspondingly, the electronic conductivities at room temperature are calculated to be $6.67 \times 10^{-8} \text{ S cm}^{-1}$ for $\text{Na}_3\text{Zr}_2\text{Si}_2\text{PO}_{12}$ and $5.23 \times 10^{-8} \text{ S cm}^{-1}$ for $\text{Na}_3\text{Zr}_2\text{Si}_2\text{PO}_{12-0.2}\text{Bi}$.

To investigate the effects of the Bi_2O_3 addition on the Na^+ transport carrier of $\text{Na}_3\text{Zr}_2\text{Si}_2\text{PO}_{12}$ electrolytes, the EIS plots of $\text{Na}_3\text{Zr}_2\text{Si}_2\text{PO}_{12}$ and $\text{Na}_3\text{Zr}_2\text{Si}_2\text{PO}_{12-0.2}\text{Bi}$ at different temperatures have been measured, as shown in Figure 4a,b,d,e. Figure 4c,f depicts the Arrhenius

curve of $\text{Na}_3\text{Zr}_2\text{Si}_2\text{PO}_{12}$ and $\text{Na}_3\text{Zr}_2\text{Si}_2\text{PO}_{12}\text{-}0.2\text{Bi}$, respectively. The activation energy E_a of the $\text{Na}_3\text{Zr}_2\text{Si}_2\text{PO}_{12}\text{-}0.2\text{Bi}$ sample at 228–373 K is 0.28 eV, which is much smaller than that of $\text{Na}_3\text{Zr}_2\text{Si}_2\text{PO}_{12}$ (0.31 eV), which is in line with the previously reported E_a value (0.26–0.40 eV) [32]. The reduced activation energy of the $\text{Na}_3\text{Zr}_2\text{Si}_2\text{PO}_{12}\text{-}0.2\text{Bi}$ samples suggests that the addition of Bi_2O_3 is feasible for Na^+ transport [30].

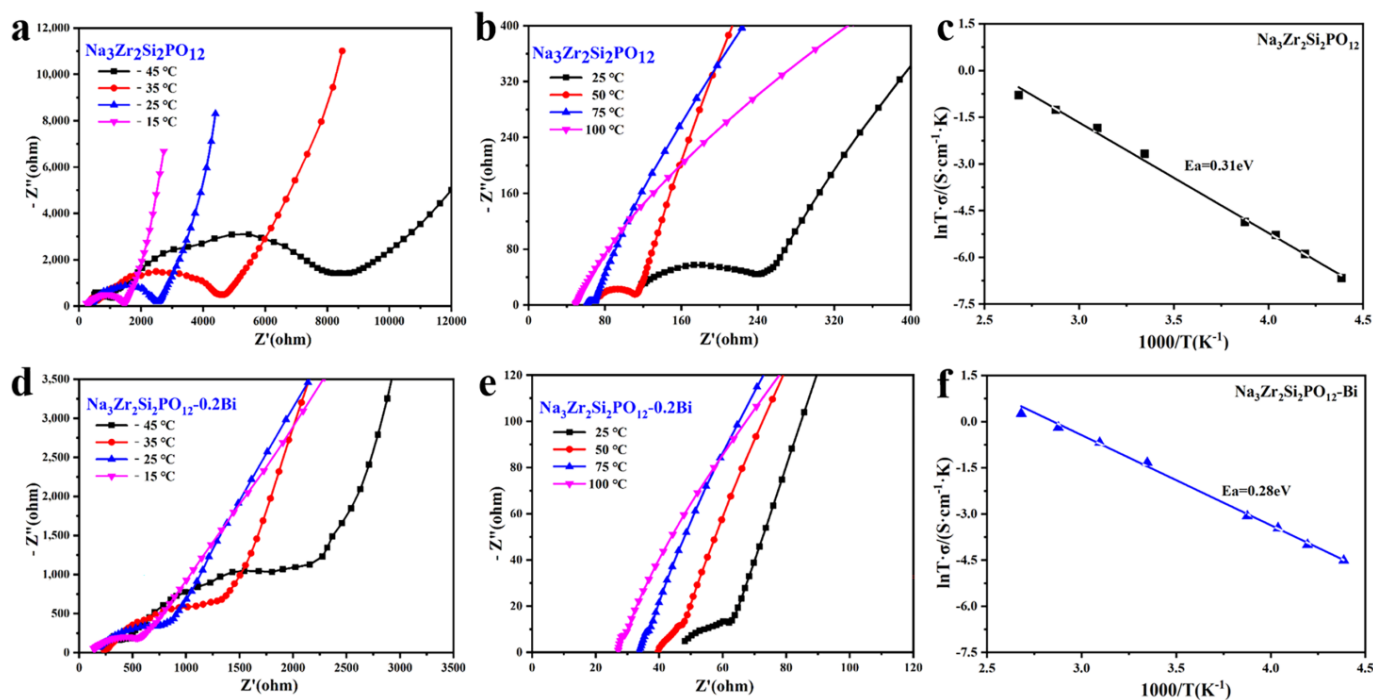


Figure 4. (a,b) Low-temperature, room-temperature and high-temperature Nyquist plots of $\text{Na}_3\text{Zr}_2\text{Si}_2\text{PO}_{12}$ electrolyte. (c) Arrhenius plot of $\text{Na}_3\text{Zr}_2\text{Si}_2\text{PO}_{12}$ electrolyte. (d,e) Low-temperature, room-temperature and high-temperature Nyquist plots of $\text{Na}_3\text{Zr}_2\text{Si}_2\text{PO}_{12}\text{-}0.2\text{Bi}$ electrolyte. (f) Arrhenius plot of $\text{Na}_3\text{Zr}_2\text{Si}_2\text{PO}_{12}\text{-}0.2\text{Bi}$ electrolyte.

To investigate the Na plating/stripping behavior, the $\text{Na}/\text{Na}_3\text{Zr}_2\text{Si}_2\text{PO}_{12}/\text{Na}$ and $\text{Na}/\text{Na}_3\text{Zr}_2\text{Si}_2\text{PO}_{12}\text{-}0.2\text{Bi}/\text{Na}$ symmetrical batteries were assembled. Critical current density (CCD) is a critical parameter to evaluate the tolerance of Na dendrite growth [33]. As shown in Figure 5a,b, the CCD of the $\text{Na}/\text{Na}_3\text{Zr}_2\text{Si}_2\text{PO}_{12}/\text{Na}$ symmetric cell is 0.35 mA cm^{-2} , which is slightly higher than that of $\text{Na}/\text{Na}_3\text{Zr}_2\text{Si}_2\text{PO}_{12}\text{-}0.2\text{Bi}/\text{Na}$ (0.30 mA cm^{-2}). The decrease of CCD after Bi_2O_3 introduction originates from the spontaneous reaction of Na with Bi^{3+} of $\text{Na}_3\text{Zr}_2\text{Si}_2\text{PO}_{12}\text{-}0.2\text{Bi}$, which would induce the formation of a Na-Bi alloy and thereupon accelerate the dendrite growth [34–36]. After CCD tests, the symmetrical batteries were disassembled (Figure 5c). Conspicuously, the large area of the black region can be observed. The $\text{Na}/\text{Na}_3\text{Zr}_2\text{Si}_2\text{PO}_{12}\text{-}0.2\text{Bi}/\text{Na}$ pellet was then ground into powder, and the corresponding XRD pattern can further confirm the existence of trace amount of Bi metal (Figure 5d).

Finally, we assembled solid sodium full batteries, using $\text{Na}_3\text{Zr}_2\text{Si}_2\text{PO}_{12}$ and $\text{Na}_3\text{Zr}_2\text{Si}_2\text{PO}_{12}\text{-}0.2\text{Bi}$ as an electrolyte and commercial $\text{Na}_3\text{V}_2(\text{PO}_4)_3$ as a cathode. For $\text{Na}_3\text{V}_2(\text{PO}_4)_3/\text{Na}_3\text{Zr}_2\text{Si}_2\text{PO}_{12}/\text{Na}$ and $\text{Na}_3\text{V}_2(\text{PO}_4)_3/\text{Na}_3\text{Zr}_2\text{Si}_2\text{PO}_{12}\text{-}0.2\text{Bi}/\text{Na}$, the initial discharging capacities were 96.8 mA h g^{-1} and 96.1 mA h g^{-1} , with initial coulombic efficiencies of 91.1% and 94.1%, respectively (Figure 5e). After 100 cycles, $\text{Na}_3\text{V}_2(\text{PO}_4)_3/\text{Na}_3\text{Zr}_2\text{Si}_2\text{PO}_{12}/\text{Na}$ and $\text{Na}_3\text{V}_2(\text{PO}_4)_3/\text{Na}_3\text{Zr}_2\text{Si}_2\text{PO}_{12}\text{-}0.2\text{Bi}/\text{Na}$ maintain reversible capacities of 95.5 mA h g^{-1} and 92.4 mA h g^{-1} with capacity retentions of 98.66% and 96.15%, respectively. Although the addition of Bi_2O_3 into an $\text{Na}_3\text{Zr}_2\text{Si}_2\text{PO}_{12}$ electrolyte can increase the relative density/ionic conductivity and decrease the electronic conductivity, it does not manifest a positive effect on the electrochemical performance of symmetrical and full batteries due to the formation of Na-Bi alloys at the Na/electrolyte interface. Such Na-Bi alloys would promote the Na

dendrite growth and further penetrate through the electrolyte. However, due to its benefits of enhanced ionic conductivity, decreased electronic conductivity and bulk density, we believe the extra interfacial modifying layer on a $\text{Na}_3\text{Zr}_2\text{Si}_2\text{PO}_{12}$ -0.2Bi surface, which acts as a physical shield so as to avoid the direct contact of Na with Bi^{3+} , can improve the electrochemical performance of $\text{Na}_3\text{Zr}_2\text{Si}_2\text{PO}_{12}$ -0.2Bi-based solid sodium metal batteries.

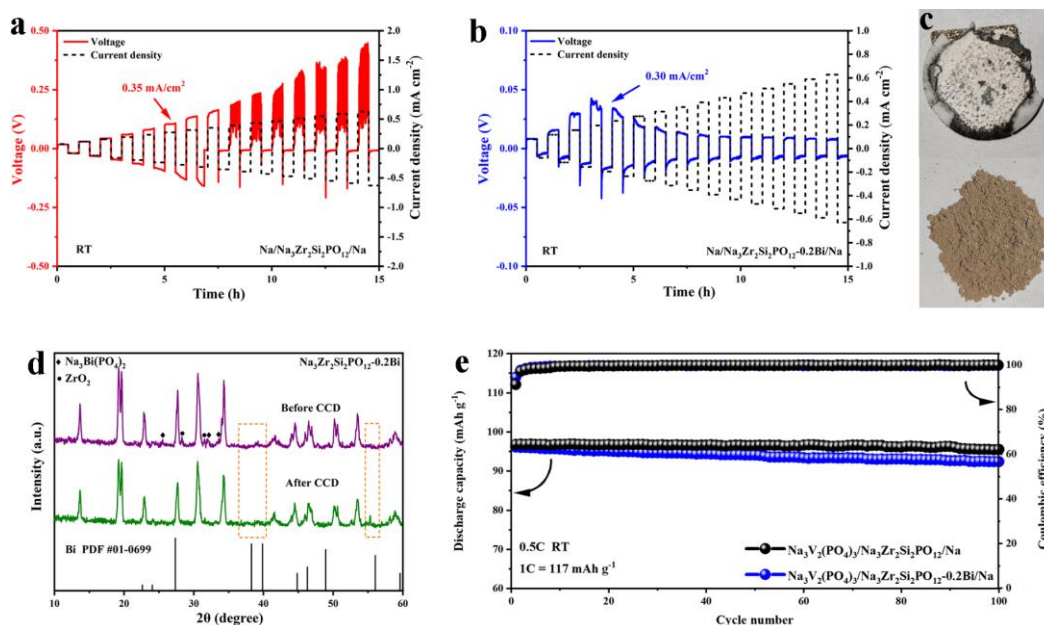


Figure 5. Critical current density of (a) Na/Na₃Zr₂Si₂PO₁₂/Na and (b) Na/Na₃Zr₂Si₂PO₁₂-0.2Bi/Na symmetrical cells at different current densities at room temperature. (c) Disassembled Na/Na₃Zr₂Si₂PO₁₂-0.2Bi/Na symmetrical battery and (d) corresponding XRD pattern of Na/Na₃Zr₂Si₂PO₁₂-0.2Bi/Na symmetrical battery after grinding. (e) Cycling performance of Na₃V₂(PO₄)₃/Na₃Zr₂Si₂PO₁₂/Na and Na₃V₂(PO₄)₃/Na₃Zr₂Si₂PO₁₂-0.2Bi/Na solid sodium full battery.

4. Conclusions

In this work, the Na₃Zr₂Si₂PO₁₂ electrolyte is prepared by a Bi₂O₃-assisted high-temperature solid-state reaction. At high temperatures, liquid Bi₂O₃ flux can prompt a relative dense microstructure of Na₃Zr₂Si₂PO₁₂ by bonding the grain. Meanwhile, the presence of Na₃Bi(PO₄)₂ impurities can enhance the Si/P ratio of Na₃Zr₂Si₂PO₁₂ and the Na⁺ occupancy, thus increasing the ionic conductivity of the Na₃Zr₂Si₂PO₁₂ electrolyte. The optimized Na₃Zr₂Si₂PO₁₂-0.2Bi electrolyte manifests an ionic conductivity of $1.27 \times 10^{-3} \text{ S cm}^{-1}$ at room temperature and a low activation energy of 0.28 eV. Despite these, due to the spontaneous reaction of Na and Bi³⁺ when assembling solid-state symmetrical and full batteries, the Bi₂O₃ introduction cannot further enhance the electrochemical performance.

Author Contributions: Conceptualization, S.C. and W.M.; methodology, X.X. and Y.Z.; writing—review and editing, Z.M. and D.W.; supervision, J.C. and C.D.; All authors have read and agreed to the published version of the manuscript.

Funding: This research was financial supported by the National Natural Science Foundation of China (Grant No. 52202282) and Scientific Developing Foundation of Tianjin Education Commission (Grant No. 2018ZD09).

Institutional Review Board Statement: Not applicable.

Informed Consent Statement: Not applicable.

Data Availability Statement: Not applicable.

Conflicts of Interest: The authors declare no conflict of interest.

References

1. Yabuuchi, N.; Kubota, K.; Dahbi, M.; Komaba, S. Research Development on Sodium-Ion Batteries. *Chem. Rev.* **2014**, *114*, 11636–11682. [[CrossRef](#)] [[PubMed](#)]
2. Chen, S.; Wu, C.; Shen, L.; Zhu, C.; Huang, Y.; Xi, K.; Maier, J.; Yu, Y. Challenges and Perspectives for NASICON-Type Electrode Materials for Advanced Sodium-Ion Batteries. *Adv. Mater.* **2017**, *29*, 1700431. [[CrossRef](#)] [[PubMed](#)]
3. Liu, G.; Sun, X.; Yu, X.; Weng, W.; Yang, J.; Zhou, D.; Xiao, R.; Chen, L.; Yao, X. Na₁₀SnSb₂S₁₂: A nanosized air-stable solid electrolyte for all-solid-state sodium batteries. *Chem. Eng. J.* **2021**, *420*, 127692. [[CrossRef](#)]
4. Wang, Y.; Richards, W.D.; Ong, S.P.; Miara, L.J.; Kim, J.C.; Mo, Y.; Ceder, G. Design principles for solid-state lithium superionic conductors. *Nat. Mater.* **2015**, *14*, 1026–1031. [[CrossRef](#)]
5. Gandi, S.S.; Gandi, S.; Madduluri, V.R.; Katari, N.K.; Dutta, D.P.; Ravuri, B.R. Na_{3+x}[Cr_xTi_{2-x}(PO₄)₃] glass-ceramic electrolyte: Ionic conductivity and structural correlations for different heat treating temperatures and time schedules. *Ionics* **2019**, *25*, 4179–4188. [[CrossRef](#)]
6. Leng, H.; Nie, J.; Luo, J. Combining cold sintering and Bi₂O₃-Activated liquid-phase sintering to fabricate high-conductivity Mg-doped NASICON at reduced temperatures. *J. Mater.* **2019**, *5*, 237–246. [[CrossRef](#)]
7. Hong, H.Y.P. Crystal structures and crystal chemistry in the system Na_{1+x}Zr₂Si_xP_{3-x}O₁₂. *Mater. Res. Bull.* **1976**, *11*, 173–182. [[CrossRef](#)]
8. Goodenough, J.B.; Hong, H.Y.P.; Kafalas, J.A. Fast Na⁺-ion transport in skeleton structures. *Mater. Res. Bull.* **1976**, *11*, 203–220. [[CrossRef](#)]
9. Kato, Y.; Hori, S.; Saito, T.; Suzuki, K.; Hirayama, M.; Mitsui, A.; Yonemura, M.; Iba, H.; Kanno, R. High-power all-solid-state batteries using sulfide superionic conductors. *Nat. Energy* **2016**, *1*, 16030. [[CrossRef](#)]
10. Sundar, G.S.; Suman, G.; Kumar, K.N.; Dutta, D.P.; Rao, R.B. Investigation on the applicability of high Na-ion conducting Na_{3+x}[Zr_xSc_{2-x}(PO₄)₃] glass-ceramic electrolyte for use in safer Na-ion batteries. *J. Phys. Chem. Solids* **2019**, *126*, 209–218. [[CrossRef](#)]
11. Lu, Y.; Alonso, J.A.; Yi, Q.; Lu, L.; Wang, Z.L.; Sun, C. A High-Performance Monolithic Solid-State Sodium Battery with Ca²⁺ Doped Na₃Zr₂Si₂PO₁₂ Electrolyte. *Adv. Energy Mater.* **2019**, *9*, 1901205. [[CrossRef](#)]
12. Yang, J.; Wan, H.-L.; Zhang, Z.-H.; Liu, G.-Z.; Xu, X.-X.; Hu, Y.-S.; Yao, X.-Y. NASICON-structured Na_{3.1}Zr_{1.95}Mg_{0.05}Si₂PO₁₂ solid electrolyte for solid-state sodium batteries. *Rare Met.* **2018**, *37*, 480–487. [[CrossRef](#)]
13. Zhang, Z.; Zhang, Q.; Shi, J.; Chu, Y.S.; Yu, X.; Xu, K.; Ge, M.; Yan, H.; Li, W.; Gu, L.; et al. A Self-Forming Composite Electrolyte for Solid-State Sodium Battery with Ultralong Cycle Life. *Adv. Energy Mater.* **2017**, *7*, 1601196. [[CrossRef](#)]
14. Miao, R.J.; Cao, X.G.; Wang, W.G.; Zhang, H.Y. Influence of Bi₂O₃ additive on the electrochemical performance of Na_{3.1}Y_{0.1}Zr_{1.9}Si₂PO₁₂ inorganic solid electrolyte. *Ceram. Int.* **2021**, *47*, 17455–17462. [[CrossRef](#)]
15. Chen, D.; Luo, F.; Zhou, W.; Zhu, D. Influence of Nb⁵⁺, Ti⁴⁺, Y³⁺ and Zn²⁺ doped Na₃Zr₂Si₂PO₁₂ solid electrolyte on its conductivity. *J. Alloy. Compd.* **2018**, *757*, 348–355. [[CrossRef](#)]
16. Khakpour, Z. Influence of M: Ce⁴⁺, Gd³⁺ and Yb³⁺ substituted Na_{3+x}Zr_{2-x}M_xSi₂PO₁₂ solid NASICON electrolytes on sintering, microstructure and conductivity. *Electrochim. Acta* **2016**, *196*, 337–347. [[CrossRef](#)]
17. Jolley, A.G.; Cohn, G.; Hitz, G.T.; Wachsmann, E.D. Improving the ionic conductivity of NASICON through aliovalent cation substitution of Na₃Zr₂Si₂PO₁₂. *Ionics* **2015**, *21*, 3031–3038. [[CrossRef](#)]
18. Huang, C.C.; Yang, G.M.; Yu, W.H.; Xue, C.; Zhai, Y.F.; Tang, W.P.; Hu, N.; Wen, Z.Y.; Lu, L.; Song, S.F. Gallium-substituted Nasicon Na₃Zr₂Si₂PO₁₂ solid electrolytes. *J. Alloy. Compd.* **2021**, *855*, 157501. [[CrossRef](#)]
19. Ma, Q.L.; Guin, M.; Naqash, S.; Tsai, C.L.; Tietz, F.; Guillon, O. Scandium-Substituted Na₃Zr₂(SiO₄)₂(PO₄) Prepared by a Solution Assisted Solid-State Reaction Method as Sodium-Ion Conductors. *Chem. Mater.* **2016**, *28*, 4821–4828. [[CrossRef](#)]
20. Song, S.F.; Duong, H.M.; Korsunsky, A.M.; Hu, N.; Lu, L. A Na⁺ Superionic Conductor for Room-Temperature Sodium Batteries. *Sci. Rep.* **2016**, *6*, 1–10. [[CrossRef](#)]
21. Wang, X.; Mei, W.; Chen, J.; Wang, D.; Mao, Z. Rare Earth Oxide-Assisted Sintered NASICON Electrolyte Composed of a Phosphate Grain Boundary Phase with Low Electronic Conductivity. *ACS Appl. Energy Mater.* **2022**, *5*, 777–783. [[CrossRef](#)]
22. Thirupathi, R.; Omar, S. A Strategic Co-doping Approach Using Sc³⁺ and Ce⁴⁺ toward Enhanced Conductivity in NASICON-Type Na₃Zr₂Si₂PO₁₂. *J. Phys. Chem. C* **2021**, *125*, 27723–27735. [[CrossRef](#)]
23. Heo, E.; Wang, J.E.; Yun, J.H.; Kim, J.-H.; Kim, D.J.; Kim, D.K. Improving Room Temperature Ionic Conductivity of Na_{3-x}K_xZr₂Si₂PO₁₂ Solid-Electrolytes: Effects of Potassium Substitution. *Inorg. Chem.* **2021**, *60*, 11147–11153. [[CrossRef](#)] [[PubMed](#)]
24. Ma, Q.L.; Tsai, C.L.; Wei, X.K.; Heggen, M.; Tietz, F.; Irvine, J.T.S. Room temperature demonstration of a sodium superionic conductor with grain conductivity in excess of 0.01 S cm⁻¹ and its primary applications in symmetric battery cells. *J. Mater. Chem. A* **2019**, *7*, 7766–7776. [[CrossRef](#)]
25. Shen, L.; Yang, J.; Liu, G.; Avdeev, M.; Yao, X. High ionic conductivity and dendrite-resistant NASICON solid electrolyte for all-solid-state sodium batteries. *Mater. Today Energy* **2021**, *20*, 100691. [[CrossRef](#)]
26. Oh, J.S.; He, L.; Plewa, A.; Morita, M.; Zhao, Y.; Sakamoto, T.; Song, X.; Zhai, W.; Zeng, K.; Lu, L. Composite NASICON (Na₃Zr₂Si₂PO₁₂) Solid-State Electrolyte with Enhanced Na⁺ Ionic Conductivity: Effect of Liquid Phase Sintering. *ACS Appl. Mater. Interfaces* **2019**, *11*, 40125–40133. [[CrossRef](#)]

27. Shao, Y.J.; Zhong, G.M.; Lu, Y.X.; Liu, L.L.; Zhao, C.L.; Zhang, Q.Q.; Hu, Y.S.; Yang, Y.; Chen, L.Q. A novel NASICON-based glass-ceramic composite electrolyte with enhanced Na-ion conductivity. *Energy Storage Mater.* **2019**, *23*, 514–521. [[CrossRef](#)]
28. Diouri, M.; Sadel, A.; Zahir, M.; Drache, M.; Conflant, P.; Wignacourt, J.P.; Boivin, J.C. Na₃Bi(PO₄)₂ type solid solutions; investigation of structural and electrical properties. *J. Alloy. Compd.* **1992**, *188*, 206–210. [[CrossRef](#)]
29. Cooper, K.R. Progress Toward Accurate Through-Plane Ion Transport Resistance Measurement of Thin Solid Electrolytes. *J. Electrochem. Soc.* **2010**, *157*, B1731. [[CrossRef](#)]
30. Wang, X.; Liu, Z.; Tang, Y.; Chen, J.; Wang, D.; Mao, Z. Low temperature and rapid microwave sintering of Na₃Zr₂Si₂PO₁₂ solid electrolytes for Na-Ion batteries. *J. Power Sources* **2021**, *481*, 228924. [[CrossRef](#)]
31. Sun, F.; Xiang, Y.; Sun, Q.; Zhong, G.; Banis, M.N.; Li, W.; Liu, Y.; Luo, J.; Li, R.; Fu, R.; et al. Insight into Ion Diffusion Dynamics/Mechanisms and Electronic Structure of Highly Conductive Sodium-Rich Na_{3+x}La_xZr_{2-x}Si₂PO₁₂ (0 ≤ x ≤ 0.5) Solid-State Electrolytes. *ACS Appl. Mater. Interfaces* **2021**, *13*, 13132–13138. [[CrossRef](#)] [[PubMed](#)]
32. Fuentes, R.O.; Figueiredo, F.; Marques, F.M.B.; Franco, J.I. Reaction of NASICON with water. *Solid State Ion.* **2001**, *139*, 309–314. [[CrossRef](#)]
33. He, S.; Xu, Y.; Chen, Y.; Ma, X. Enhanced ionic conductivity of an F--assisted Na₃Zr₂Si₂PO₁₂ solid electrolyte for solid-state sodium batteries. *J. Mater. Chem. A* **2020**, *8*, 12594–12602. [[CrossRef](#)]
34. Lu, Y.; Zhao, C.-Z.; Yuan, H.; Cheng, X.-B.; Huang, J.-Q.; Zhang, Q. Critical Current Density in Solid-State Lithium Metal Batteries: Mechanism, Influences, and Strategies. *Adv. Funct. Mater.* **2021**, *31*, 2009925. [[CrossRef](#)]
35. Fang, W.; Fan, L.; Zhang, Y.; Zhang, Q.; Yin, Y.; Zhang, N.; Sun, K. Synthesis of carbon coated Bi₂O₃ nanocomposite anode for sodium-ion batteries. *Ceram. Int.* **2017**, *43*, 8819–8823. [[CrossRef](#)]
36. Xu, R.; Kinderman, R.; Van der Lugt, W. Electrical resistivities of liquid Na-Bi and Rb-Bi alloys. *J. Phys. Condens. Matter* **1991**, *3*, 127–133. [[CrossRef](#)]